Subacute and chronic left ventricular myocardial scar: accuracy of texture analysis on nonenhanced cine MR images

Baessler, Bettina ; Mannil, Manoj ; Oebel, Sabrina ; Maintz, David ; Alkadhi, Hatem ; Manka, Robert

Abstract: Purpose To test whether texture analysis (TA) allows for the diagnosis of subacute and chronic myocardial infarction (MI) on noncontrast material-enhanced cine cardiac magnetic resonance (MR) images. Materials and Methods In this retrospective, institutional review board-approved study, 120 patients who underwent cardiac MR imaging and showed large transmural (volume of enhancement on late gadolinium enhancement [LGE] images >20%, n = 72) or small (enhanced volume 20%, n = 48) subacute or chronic ischemic scars were included. Sixty patients with normal cardiac MR imaging findings served as control subjects. Regions of interest for TA encompassing the left ventricle were drawn by two blinded, independent readers on cine images in end systole by using a freely available software package. Stepwise dimension reduction and texture feature selection based on reproducibility, machine learning, and correlation analyses were performed for selecting features, enabling the diagnosis of MI on nonenhanced cine MR images by using LGE imaging as the standard of reference. Results Five independent texture features allowed for differentiation between ischemic scar and normal myocardium on cine MR images in both subgroups: Teta1, Perc.01, Variance, WavEnHH.s-3, and S(5,5)SumEntrp (in patients with large MI: all P values < .001; in patients with small MI: Teta1 and Perc.01, P < .001; Variance, P = .026; WavEnHH.s-3, P = .007; S[5,5]SumEntrp, P = .045). Multiple logistic regression models revealed that combining the features Teta1 and Perc.01 resulted in the highest accuracy for diagnosing large and small MI on cine MR images, with an area under the curve of 0.93 and 0.92, respectively. Conclusion This proof-of-concept study indicates that TA of nonenhanced cine MR images allows for the diagnosis of subacute and chronic MI with high accuracy. (©) RSNA, 2017 Online supplemental material is available for this article.

DOI: https://doi.org/10.1148/radiol.2017170213

Radiology

Subacute and Chronic Left Ventricular Myocardial Scar: Accuracy of Texture Analysis on Nonenhanced Cine MR Images[1]

Bettina Baessler, MD
Manoj Mannil, MD, MSc
Sabrina Oebel, MD
David Maintz, MD
Hatem Alkadhi, MD, MPH, EBCR
Robert Manka, MD

Purpose: To test whether texture analysis (TA) allows for the diagnosis of subacute and chronic myocardial infarction (MI) on noncontrast material–enhanced cine cardiac magnetic resonance (MR) images.

Materials and Methods: In this retrospective, institutional review board–approved study, 120 patients who underwent cardiac MR imaging and showed large transmural (volume of enhancement on late gadolinium enhancement [LGE] images >20%, n = 72) or small (enhanced volume ≤20%, n = 48) subacute or chronic ischemic scars were included. Sixty patients with normal cardiac MR imaging findings served as control subjects. Regions of interest for TA encompassing the left ventricle were drawn by two blinded, independent readers on cine images in end systole by using a freely available software package. Stepwise dimension reduction and texture feature selection based on reproducibility, machine learning, and correlation analyses were performed for selecting features, enabling the diagnosis of MI on nonenhanced cine MR images by using LGE imaging as the standard of reference.

Results: Five independent texture features allowed for differentiation between ischemic scar and normal myocardium on cine MR images in both subgroups: Teta1, Perc.01, Variance, WavEnHH.s-3, and S(5,5)SumEntrp (in patients with large MI: all P values < .001; in patients with small MI: Teta1 and Perc.01, P < .001; Variance, P = .026; WavEnHH.s-3, P = .007; S[5,5]SumEntrp, P = .045). Multiple logistic regression models revealed that combining the features Teta1 and Perc.01 resulted in the highest accuracy for diagnosing large and small MI on cine MR images, with an area under the curve of 0.93 and 0.92, respectively.

Conclusion: This proof-of-concept study indicates that TA of nonenhanced cine MR images allows for the diagnosis of subacute and chronic MI with high accuracy.

Online supplemental material is available for this article.

[1] From the Institute of Diagnostic and Interventional Radiology, University Hospital Zurich, University of Zurich, Raemistrasse 100, CH-8091 Zurich, Switzerland (B.B., M.M., S.O., H.A., R.M.); Department of Radiology, University Hospital of Cologne, Cologne, Germany (B.B., D.M.); Department of Cardiology, University Heart Center Zurich, Zurich, Switzerland (S.O., R.M.); and Institute for Biomedical Engineering, University and ETH Zurich, Zurich, Switzerland (R.M.). Received February 20, 2017; revision requested April 17; revision received May 2; accepted May 16; final version accepted June 2. **Address correspondence to** H.A. (e-mail: *hatem.alkadhi@usz.ch*).

Myocardial infarction (MI) causes about one-third of all deaths in the group of patients older than 35 years (1). Patients with myocardial scar after MI are at increased risk for arrhythmia and death (2), highlighting the relevance of detecting and characterizing myocardial scar to guide intensive secondary prevention (3).

Late gadolinium enhancement (LGE) cardiac magnetic resonance (MR) imaging is a clinically established and accurate method for the assessment of ischemic myocardial scar (4,5). However, patients with coronary artery disease have a higher prevalence of coexisting chronic kidney disease compared with patients without coronary artery disease (6), which makes methods for detecting myocardial scar without the need of gadolinium administration desirable (7). In addition, intravenous administration of gadolinium-based contrast agents in patients with chronic kidney disease carries the risk for developing nephrogenic systemic sclerosis (8).

Texture analysis (TA) comprises a wide range of techniques modeling spatial distributions of pixel gray levels for recognizing, classifying, and segmenting data based on the underlying texture (9,10). Because traditional visual inspection of images might not allow for recognizing subtle differences in textural information, the application of TA has the potential to further enhance the diagnostic and prognostic value of imaging. The increase of interest in evaluating TA in radiology is reflected by recent literature describing potential applications of the technique in oncologic (11–13), neuroradiologic (14), musculoskeletal (15,16), and lung imaging (17).

To our knowledge, only one preliminary study, published as a conference abstract, has evaluated the potential of TA for cardiac MR imaging so far (18). Thus, our hypotheses for the present study are that TA is feasible when applied on noncontrast material–enhanced cine images and that TA parameters allow for the diagnosis of ischemic myocardial scar based on the texture of the myocardium on nonenhanced cine MR images. The purpose of our study was to test whether TA allows for the diagnosis of subacute and chronic MI on nonenhanced cine cardiac MR images.

Advances in Knowledge

- Five independent texture analysis (TA) features (Perc.01, Teta1, Variance, WavEnHH.s-3, and S[5,5]SumEntrp) on cine MR images showed significant differences between patients with subacute and chronic ischemic myocardial scar and control subjects.
- Combination of the TA features Perc.01 and Teta1 allowed for the diagnosis of small (enhanced volume at late gadolinium enhancement imaging ≤20%) as well as large (enhanced volume >20%) myocardial scars on nonenhanced cine MR images with excellent accuracy.
- The two best classifying TA features Perc.01 and Teta1 exhibited high intra- and interobserver reproducibility.

Materials and Methods

This study had institutional review board and local ethics committee approval. All cardiac MR imaging studies were clinically indicated. Requirement for written informed consent was waived because of the retrospective nature of the study.

Study Population

We included 120 patients (15 women; mean age ± standard deviation, 64 years ± 10) who underwent cardiac MR imaging between January and October 2016 after clinical diagnosis of MI and who had a subacute or chronic ischemic myocardial scar based on LGE imaging findings. As control subjects, we included 60 additional consecutive patients (27 women; mean age, 48 years ± 17) who had been referred during the same period and who demonstrated normal cardiac MR imaging findings. Causes for referral in the control group were as follows: exclusion of structural heart disease (n = 29); exclusion of heart disease in subjects with known familial predisposition to inheritable cardiomyopathy, that is, known family history of hypertrophic cardiomyopathy or arrhythmogenic right ventricular dyplasia (n = 10); and exclusion of myocardial perfusion deficits (n = 21). Inclusion criteria for the control subjects were as follows: absence of known cardiac or systemic disease, no history of previous cardiac surgery or intervention, normal cardiac dimensions and function based on cine cardiac MR imaging findings, absence of edematous signal alterations at T2-weighted imaging, and absence of contrast enhancement at LGE imaging. Demographics and left ventricular (LV) volumetric data of patients and control subjects are summarized in Table 1.

Implication for Patient Care

- TA based on nonenhanced cine MR images allows for the diagnosis of subacute and chronic ischemic myocardial scar without the need for gadolinium-enhanced imaging, which could be relevant in patients with concomitant chronic kidney disease who are at increased risk for gadolinium-associated complications.

Cardiac MR Imaging Data Acquisition

Cardiac MR imaging examinations were performed by using a 1.5-T clinical system

https://doi.org/10.1148/radiol.2017170213

Content code: CA

Radiology 2017; 000:1–10

Abbreviations:
LGE = late gadolinium enhancement
LV = left ventricle
MI = myocardial infarction
TA = texture analysis

Author contributions:
Guarantors of integrity of entire study, B.B., H.A.; study concepts/study design or data acquisition or data analysis/interpretation, all authors; manuscript drafting or manuscript revision for important intellectual content, all authors; approval of final version of submitted manuscript, all authors; agrees to ensure any questions related to the work are appropriately resolved, all authors; literature research, B.B., H.A., R.M.; clinical studies, B.B., M.M., S.O., H.A., R.M.; statistical analysis, B.B., D.M., H.A.; and manuscript editing, B.B., M.M., D.M., H.A., R.M.

Conflicts of interest are listed at the end of this article.

Table 1

Patient Demographics

Parameter	Control Subjects ($n = 60$)	Patients with MI (Entire Cohort, $n = 120$)	Small MI Patient Subgroup ($n = 42$)	Large MI Patient Subgroup ($n = 78$)
Age (y)	48 ± 17	64 ± 10*	66 ± 9*	63 ± 10*
Height (cm)	170 ± 10	172 ± 8	174 ± 9	172 ± 8
Weight (kg)	73 ± 17	81 ± 15†	81 ± 14‡	80 ± 15‡
LV end diastolic volume (mL)	146 ± 34	176 ± 54*	165 ± 58	183 ± 51*
LV end systolic volume (mL)	59 ± 18	96 ± 47*	83 ± 44†§	103 ± 48*‖
LV ejection fraction (%)	60 ± 5	48 ± 20*	52 ± 10*#	45 ± 12***
LV stroke volume (mL)	87 ± 19	80 ± 20‡	82 ± 22	79 ± 20
LV end diastolic wall mass/body surface area (g/m^2)	48 ± 10	64 ± 16*	63 ± 14*	64 ± 17*
LGE myocardial volume (%)	…	27.2 ± 12.9	13.6 ± 4.2††	34.7 ± 9.5‡‡

Note.—Data are means ± standard deviation.

* $P < .001$ when compared with control subjects.

† $P < .01$ when compared with control subjects.

‡ $P < 0.5$ when compared with control subjects.

§ $P < .05$ when compared with large MI patient subgroup.

‖ $P < .05$ when compared with small MI patient subgroup.

# $P < .01$ when compared with large MI patient subgroup.

** $P <$. 01 when compared with small MI patient subgroup.

†† $P < .001$ when compared with large MI patient subgroup.

‡‡ $P < .001$ when compared with small MI patient subgroup.

(Achieva; Philips Healthcare, Best, the Netherlands) with a standard five-element cardiac phased-array coil. A balanced steady-state free precession cine sequence with breath-hold technique and retrospective electrocardiography triggering was performed in short-axis orientation for functional analysis of the LV and subsequent TA. A detailed description of the protocol parameters is provided in Table E1 (online). Edema imaging was performed with a standard T2-weighted double-inversion black-blood spin-echo sequence in three short-axis sections. For the depiction of myocardial scar, LGE images covering the entire LV were acquired 15 minutes after administration of a bolus of 0.2 mmol of gadobutrol (Gadovist; Bayer Schering, Berlin, Germany) per kilogram of body weight by using an inversion recovery gradient-echo MR imaging sequence.

Cardiac MR Imaging Data Analysis and Patient Subgroups

LV volumetric analysis was performed by using commercially available software (Extended MR Workspace, version 2.6.3.4; Philips Healthcare). Patients with recent or acute MI identified by the presence of edema were excluded to avoid confounding effects of edema on cine MR images on TA features. Therefore, T2-weighted images were assessed visually for regions with elevated signal intensity indicating myocardial edema, and patients with edema were excluded from further analyses. LGE images were assessed visually for the presence of contrast enhancement with a typical ischemic (subendocardial or transmural) pattern.

The volume of MI was then quantified by one reader (M.M., with 5 years of experience in cardiovascular imaging) on LGE images with a semiautomatic approach by using commercially available software (IntelliSpace Portal, version 7.0; Philips Healthcare). Endocardial and epicardial contours were manually traced and the areas of hyperenhancing myocardium were automatically segmented by using 5 standard deviations above the average signal in the normal myocardium as previously shown (19). The threshold could be manually overridden for a specific location to exclude obvious artifacts. After segmentation, myocardial and fibrous tissue mass was calculated.

Patients were then further subdivided into two groups according to the size of myocardial scar with a threshold of the percentage of enhanced myocardial volume on LGE images of less than or equal to 20% indicating small myocardial scar ($n = 42$; five women; mean age, 66 years ± 9) and greater than 20% indicating large myocardial scar ($n = 78$; 10 women; mean age, 63 years ± 10), based on previous work showing an association of scar size with adverse cardiac events (20).

Texture Analysis

TA represents a statistical image analysis technique that quantifies the texture of an image on the basis of pixel signal intensity distributions and relationships of values between neighboring pixels (16). Generally speaking, textures are complex patterns composed of entities or subpatterns that have characteristic brightness, slope, size, et cetera. Texture can be regarded as a similarity grouping in an image. The local subpattern properties give rise to the perceived lightness, uniformity, density, roughness, regularity, linearity, and many other properties of the texture as a whole (21).

TA was performed in all 180 patients by a radiologist (B.B., with 5 years of experience in cardiovascular imaging) using a freely available software package (MaZda, version 4.6; Institute of Electronics, Technical University of Lodz, Lodz, Poland) (22) installed on a standard personal computer. In control subjects, a midventricular section was used for analyses. In patients, a single cine section demonstrating the largest region of LGE was chosen. After selection of single cine sections, a single image in a Digital Imaging and Communications in Medicine, or DICOM, format was exported for further analysis, displaying only the end-systolic phase of the heart cycle to allow for a subsequent blinded analysis. In addition, images of all patients and control subjects were randomized with respect to

Figure 1

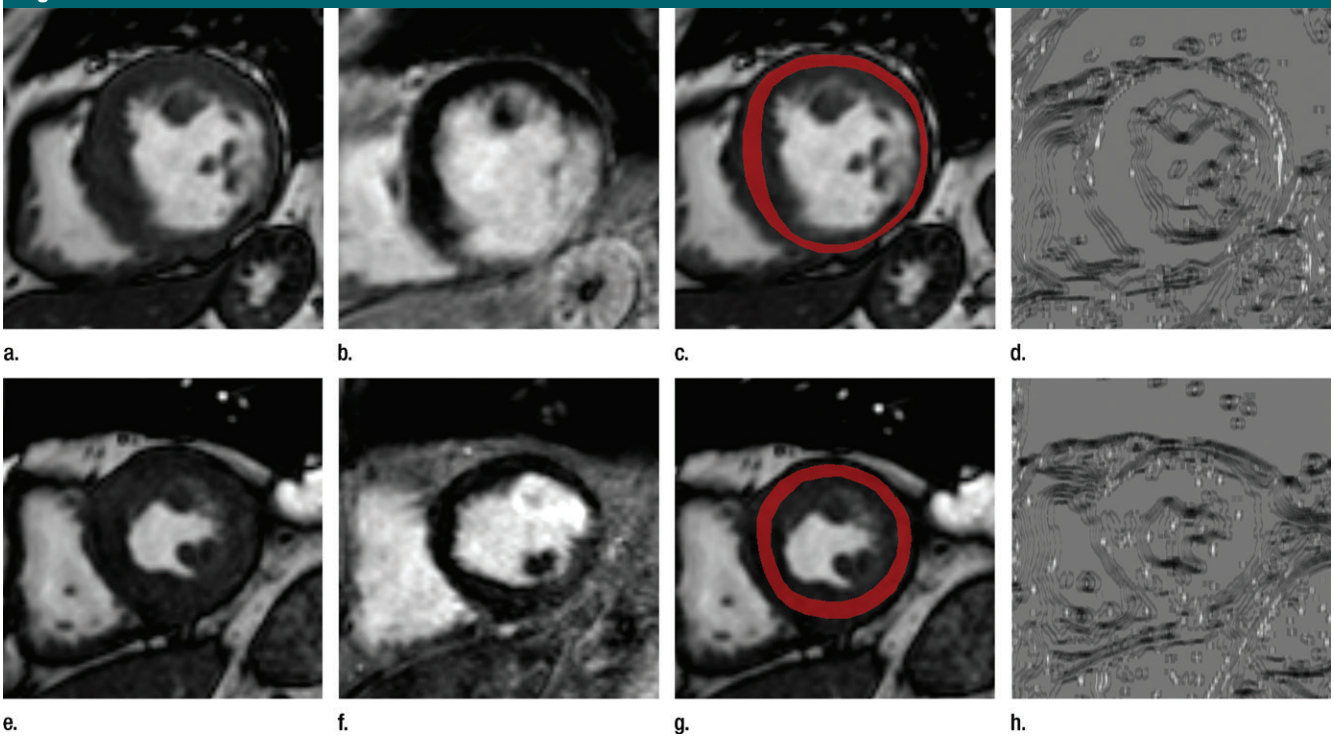

Figure 1: **(a, e)** Cine images with corresponding **(b, f)** LGE images, **(c, g)** regions of interest (red circle) for TA, and **(d, h)** parametric map of texture feature Teta1 in a 72-year-old man (patient subgroup with large myocardial scar; upper row) with transmural infarction and signal abnormalities on cine MR images and a 68-year-old man (patient subgroup with small myocardial scar; bottom row) with small subendocardial infarction without signal abnormalities on cine MR images.

the presence or absence of LGE. After 2 weeks, regions of interest encompassing the LV myocardium were drawn on these end-systolic cine images (Fig 1). The trabeculated layer and epicardial border were carefully excluded to avoid partial volume effects. Drawing of regions of interest and computation of the TA features by the software took about 40 seconds per patient.

For testing the intra- and interobserver reproducibility of texture features, region of interest delineation was repeated twice in a subset of 30 subjects (10 control subjects, 10 patients with large MI, and 10 patients with small MI) by the same reader for intraobserver analysis and by a second radiologist (M.M.) for interobserver analysis.

Gray-level normalization was performed with the TA software by rescaling the histogram data to fit within μ-gray-level mean ± 3σ (σ-gray-level standard deviation) to minimize the effect of brightness and contrast variations on TA (23). Five subset texture feature sets were extracted separately (Table 2), resulting in a total of 286 texture features.

Texture Feature Selection and Dimension Reduction

Because of the high number of texture features, feature selection and dimension reduction were necessary to reduce the feature set to those that contributed most to classification accuracy (24). In a first step, texture features with low reproducibility were excluded from further analyses for selecting only clinically useful parameters. Intra- and interobserver reproducibility of all extracted texture features were assessed by calculating intraclass correlation coefficients, and all features with an intraclass correlation coefficient of less than 0.75 (with those ranging from 0.75 to 1 considered "excellent" [25]) were excluded.

The remaining features were analyzed by using machine learning algorithms to achieve further dimension reduction. Analyses were performed in R (version 3.1.2; R Foundation, Vienna, Austria) (26) by using the packages Boruta (27) and caret (28). Two-dimension reduction algorithms were used independently to internally validate the variable selection process. The Boruta algorithm uses a random forest algorithm and performs a top-down search for relevant features by comparing the importance of original attributes with the importance of those achievable at random and progressively eliminates irrelevant features to stabilize the model (27). In recursive feature elimination, a random forest algorithm is used for each iteration to evaluate the model. The algorithm is configured to explore all possible subsets of the attributes and finally selects the most important variables for an optimal model fit.

Table 2

Overview of All Computed Texture Categories with Corresponding Features

Texture Category	Texture Feature
Histogram	Mean, variance, skewness, kurtosis, percentiles (1%, 10%, 50%, 90%, 99%)
Co-occurrence matrix (computed for four directions [(a,0), (0,a), (a,a), (0,-a)] at five interpixel distances (a = 1–5)	Angular second moment, contrast, correlation, entropy, sum entropy, sum of squares, sum average, sum variance, inverse different moment, difference entropy, difference variance
Run-length matrix (computed for four angles [vertical, horizontal, 0°, and 135°])	Run-length nonuniformity, gray-level nonuniformity, long run emphasis, short run emphasis, fraction of image in runs
Absolute gradient	Gradient mean, variance, skewness, kurtosis, and nonzeros
Autoregressive model	Teta1 to 4, sigma
Wavelet transform (calculated for four subsampling factors (n = 1–4)	Energy of wavelet coefficients in low-frequency subbands, horizontal high-frequency subbands, vertical high-frequency subbands, and diagonal high-frequency subbands

Statistical Analysis

R packages used for further statistical analyses are described in Appendix E1 (online). All continuous data are given as means ± standard deviation. A two-tailed P value of $< .05$ was considered to indicate statistical significance. Testing for group differences was performed by using independent t tests after assessing normal distribution of the data. For multiple group comparisons, analysis of variance testing with Tukey-type comparisons was performed.

For selecting variables that allow classification of patients from control subjects and for patient subgroup analyses, multiple and multinomial logistic regression models were fitted and compared by using the Akaike Information Criterion. The misclassification rate of these models was assessed by using 10-fold cross validation. The diagnostic accuracy of optimal predictive parameters was evaluated from the area under the curve from receiver operating characteristic analyses, and diagnostic sensitivity and specificity were calculated. For excluding a confounding influence of wall thickness and associated partial volume effects on texture parameters, Pearson correlation analyses were performed between the LV wall mass and the identified, relevant texture features. Intra- and interobserver agreement was tested by using intraclass correlation coefficients and Bland-Altman analyses.

Results

Texture Feature Selection

Texture feature selection was performed on the entire dataset (120 patients and 60 control subjects). The first step based on calculation of intraclass correlation coefficients for intra- and interreader reproducibility led to the exclusion of 80 texture features. The remaining 206 features were independently fed into the two distinct dimension-reduction and feature-elimination algorithms, resulting in the selection of the same 26 features (Table E2 [online]). Figure E1 (online) shows the graphical output of the Boruta-based feature selection process. Because both dimension-reduction algorithms do not account for collinearity in the data, a correlation matrix was calculated for the 26 most important variables to detect highly collinear texture features (Fig 2). Of the highly correlated parameters (defined as Pearson r ≥0.6), only one from each cluster with the highest Gini index in a random forest model separately fitted on the 26 most important variables was selected for further analyses (texture parameters in Table E2 [online]). At the end of the multistep dimension reduction process, the five most important and independent texture features were selected for further statistical analyses, including two first-order texture features (Perc.01, Variance), one second-order feature (S[5,5]SumEntrp), and two higher-order features (Teta1, WavEnHH.s-3).

Texture Features Diagnosing Scar on Cine MR Images

Comparing all patients with MI and control subjects, all five texture features showed significant differences between groups (Table 3). In multiple logistic regression analyses, a model containing the two parameters Teta1 and Perc.01 proved to be the best for differentiating between patients with MI and control subjects according to the Akaike Information Criterion. In 10-fold cross validation, this model yielded an internal estimate of accuracy of 0.84 and a cross-validation estimate of accuracy of 0.84. The logistic regression analysis showed a sensitivity of 86% and a specificity of 82% (Table 4). The combination of Teta1 and Perc.01 resulted in the highest area under the curve of 0.92 when compared with Teta1 (0.88) and Perc.01 alone (0.80).

In correlation analyses, a weak correlation was observed between the texture features and LV wall mass (r = 0.32 for Teta1 vs indexed LV wall mass and r = −0.22 for Perc.01 vs indexed LV wall mass).

Texture Features Diagnosing Myocardial Scar in the Subgroups

Similar to the entire patient cohort, the same five texture features showed significant differences between the subgroup with large myocardial scar (LGE >20%) and control subjects (Fig 3, Table 3). None of the five texture features allowed for a significant differentiation between large and small MI in the two subgroups (Fig 3, Table 3).

In multinomial logistic regression analyses, a model containing the two parameters Teta1 and Perc.01 proved

Figure 2

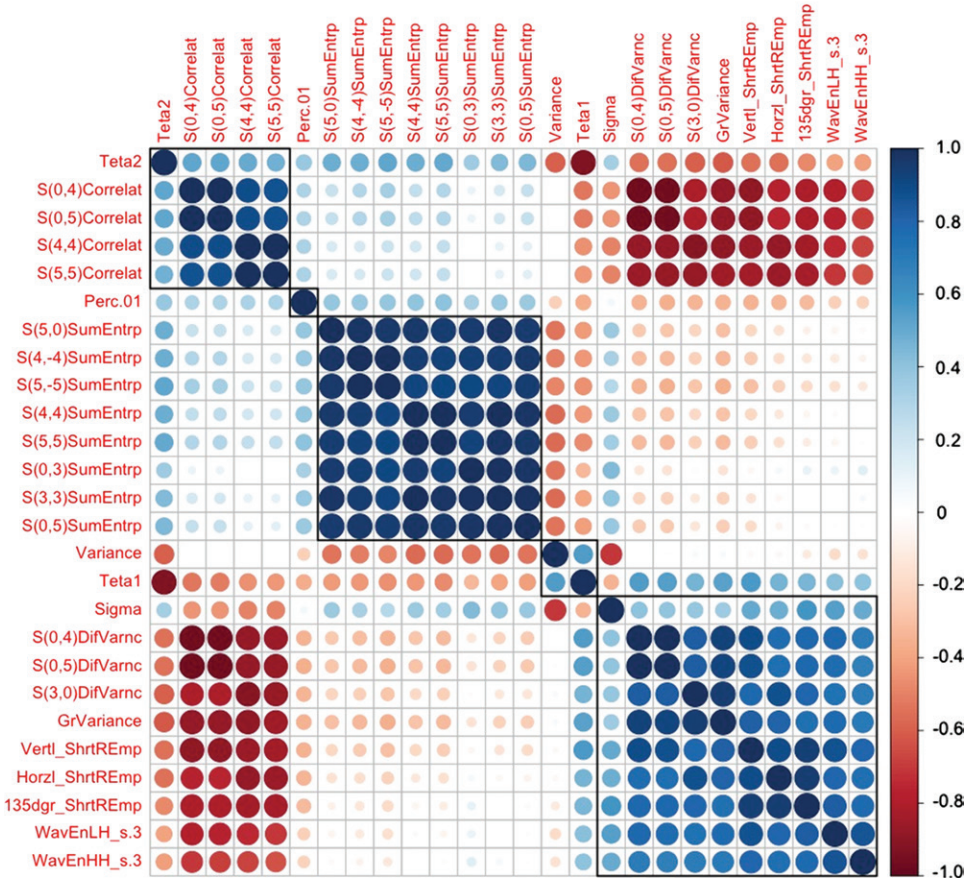

Figure 2: Correlogram illustrates auto- and cross-correlations of 26 most important texture features. Texture features were reordered after hierarchical clustering for visualizing different feature clusters. Five clusters of texture features became apparent (rectangular boxes). Blue circles indicate positive correlation and red circles indicate negative correlation. The larger the circle and the darker the color, the higher is the correlation between two variables.

to be the best for differentiating between control subjects and patients with large myocardial scar and between control subjects and patients with small myocardial scar according to the Akaike Information Criterion. A 10-fold cross validation resulted in an internal estimate of accuracy of 0.89 and a cross-validation estimate of accuracy of 0.81 for patients with large myocardial scar versus control subjects, and an internal estimate of accuracy of 0.77 and a cross-validation estimate of accuracy of 0.75 for patients with small myocardial scar versus control subjects. Diagnostic sensitivity and specificity for differentiating between control subjects and patients with large and patients with small myocardial scar, as well as corresponding areas under the curve from receiver operating characteristic analyses, are shown in Table 4 and Figure 4.

Reproducibility of Important Texture Features

Intra- and interobserver reproducibility of the two best classifying features Teta1 and Perc.01 was excellent (intraobserver intraclass correlation coefficient: 0.938 for Perc.01 and 0.952 for Teta1; interobserver intraclass correlation coefficient: 0.873 for Perc.01 and 0.980 for Teta1). Bland-Altman analyses showed narrow limits of agreement for both texture features on the intra- and interobserver level (Fig 5).

Discussion

TA models spatial distributions of pixel gray levels and allows for the analysis and classification of medical imaging data according to different tissue textures (9,10), thus offering the potential to overcome limitations of a pure visual image interpretation. Previous studies reporting on regional myocardial lipomatous metaplasia leading to chemical shift artifacts (29), wall thinning, and/or wall motion abnormalities in regions of myocardial scar (30) suggested that it might be feasible to depict ischemic scars on cine MR images alone. However, accurate identification of ischemic myocardial scars is possible only when also analyzing corresponding LGE

Table 3

Differences of Selected Texture Features between Patients with MI and Control Subjects

Parameter	Control Subjects ($n = 60$)	Patients with MI (Entire Cohort, $n = 120$)	Small MI Patient Subgroup ($n = 42$)	Large MI Patient Subgroup ($n = 78$)
Teta1	0.74 ± 0.05*†‡	0.84 ± 0.07§	0.82 ± 0.05§	0.85 ± 0.07§
Perc.01	21.1 ± 9.2*†‡	10.5 ± 9.1§	11 ± 9§	10.4 ± 9.2§
Variance	44 ± 32*†‡	93 ± 80§	80 ± 51§	99 ± 92§
WavEnHH.s-3	0.039 ± 0.033*†‡	0.080 ± 0.061§	0.070 ± 0.064§	0.084 ± 0.064§
S(5,5)SumEntrp	1.24 ± 0.03*†‡	1.20 ± 0.07§	1.22 ± 0.06§	1.19 ± 0.08§

Note.—Data are means ± standard deviation.

* $P < .001$ when compared with all patients with MI.

† $P < .001$ when compared with small MI patient subgroup.

‡ $P < .001$ when compared with large MI patient subgroup.

§ $P < .001$ when compared with control subjects.

Table 4

Sensitivity, Specificity, and AUC of the Best Logistic Regression Model (Teta1 and Perc.01) for Differentiating between Patients, Patient Subgroups, and Control Subjects

Patient Group	Sensitivity (%)	Specificity (%)	AUC
All patients with MI ($n = 120$)	86	82	0.92
Subgroup with small myocardial scar ($n = 42$)	83	82	0.92
Subgroup with large myocardial scar ($n = 78$)	91	78	0.93

Note.—AUC = area under the curve.

images, which holds true particularly for small ischemic scars.

Our proof-of-concept study indicated that TA is feasible and reproducible on cine MR images and delivers texture parameters, which allow for an accurate differentiation between control subjects and patients with both large and small subacute and chronic myocardial scars.

We computed texture features from the entire LV myocardium instead of matching regions of interest to areas of contrast enhancement on LGE images or wall motion abnormalities. Aiming at a reproducible and standardized approach toward detection of myocardial scars without gadolinium administration, this approach for region of interest delineation is also potentially suitable for clinical routine, in which myocardial scars might not be visualized on cine MR images. Nevertheless, a segmental approach to region of interest delineation would also be interesting to further differentiate between segments demonstrating myocardial scar and those with remote myocardium. Future studies might then be able to compare a segment-based approach with an approach including the entire myocardium in the region of interest as proposed in the present study.

One of the main challenges with TA is the huge amount of available texture features, which can be computed from a single region of interest. By using a freely available and widely used software package (22), our study included a total of 286 features. After excluding less reproducible features, we obtained 206 texture features. We assumed that the intra- and interobserver variability was related to how LV borders were manually traced by the two readers. The next step in feature reduction was based on advanced statistical methods including machine learning (31,32). Two other approaches for feature reduction have been recently suggested: averaging texture features among different directions (16) or using more advanced machine learning algorithms such as neuronal networks or deep learning, leading the path to the field of radiomics (33).

Because especially small transmural and subendocardial scars often show no signal abnormalities on cine MR images and therefore represent a major challenge for a diagnosis based on nonenhanced imaging findings, we divided our patients with MI into two subgroups. In both subgroups with small and large transmural ischemic scars, we found that TA is able to differentiate between normal myocardium and scar with excellent accuracy. Hence, TA offers the potential to represent a potential alternative to LGE imaging, which could be of interest in patients with chronic kidney disease in whom gadolinium administration should be avoided.

The most important texture feature for detecting ischemic scar on cine MR images in our study was Teta1. Teta1 represents a higher-order feature derived from the autoregressive model, which provides information about local interactions between neighboring pixels with respect to their gray-level values (9) and has been previously reported to allow for the discrimination of patterns in MR images (34). The combination of Teta1 with the first-order feature Perc.01 led to a further increase in accuracy, indicating the benefit of combining two texture features in classification models for improving the diagnosis. Because we observed only a weak correlation of the two texture features with LV wall thickness, we believe that it is the myocardial texture rather than partial volume effects caused by wall thinning leading to the excellent discrimination between the different patient groups.

Despite the ability to differentiate between control subjects and patients, none of the five texture features was able to differentiate between the two patient subgroups. Further studies

Figure 3

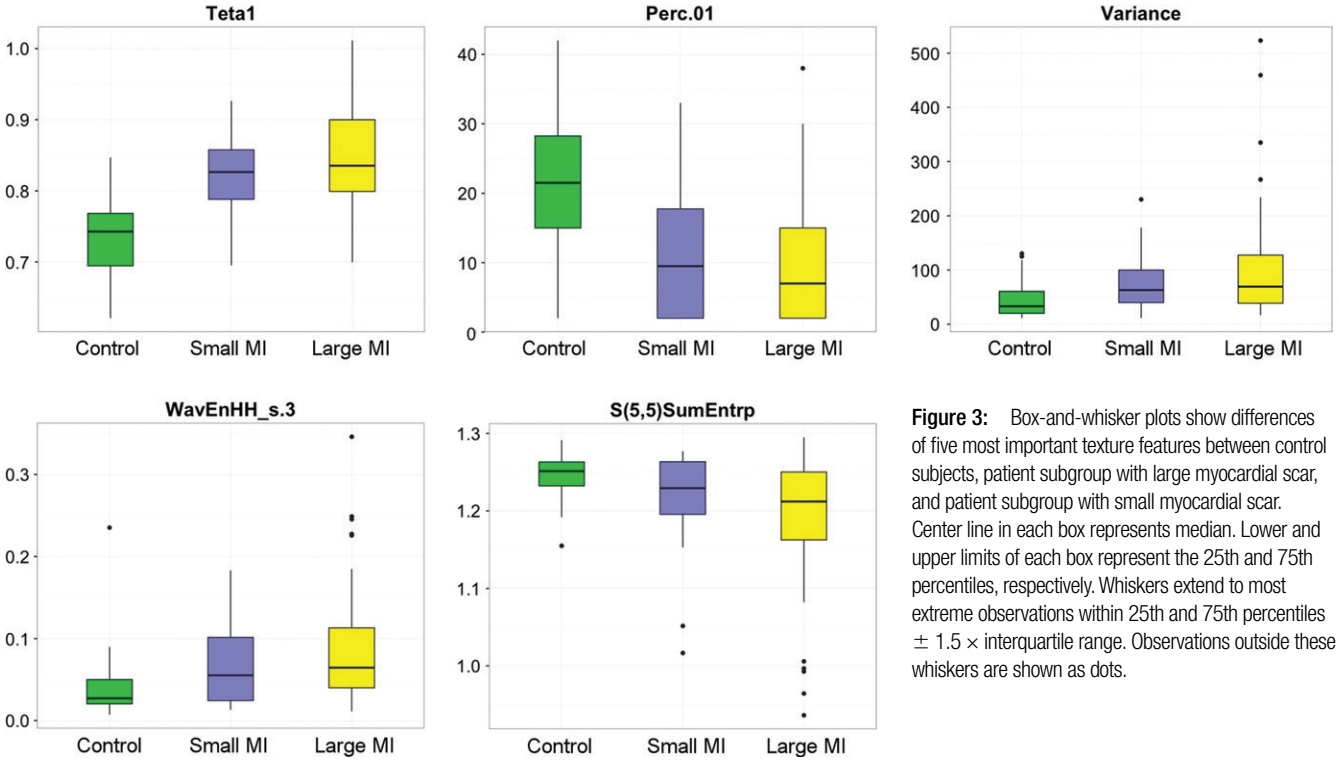

Figure 3: Box-and-whisker plots show differences of five most important texture features between control subjects, patient subgroup with large myocardial scar, and patient subgroup with small myocardial scar. Center line in each box represents median. Lower and upper limits of each box represent the 25th and 75th percentiles, respectively. Whiskers extend to most extreme observations within 25th and 75th percentiles ± 1.5 × interquartile range. Observations outside these whiskers are shown as dots.

Figure 4

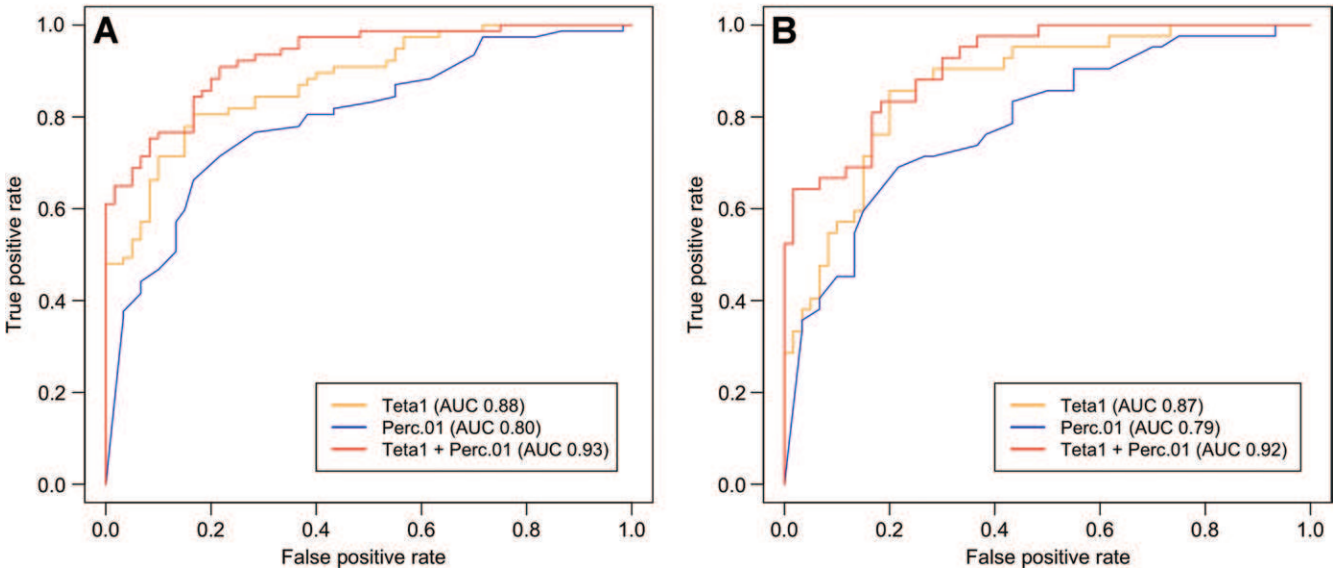

Figure 4: Graphs show receiver operating characteristic analysis indicating accuracy of TA features for diagnosing ischemic myocardial scars in, *A,* patient subgroup with large myocardial scar and, *B,* in patient subgroup with small myocardial scar.

Figure 5

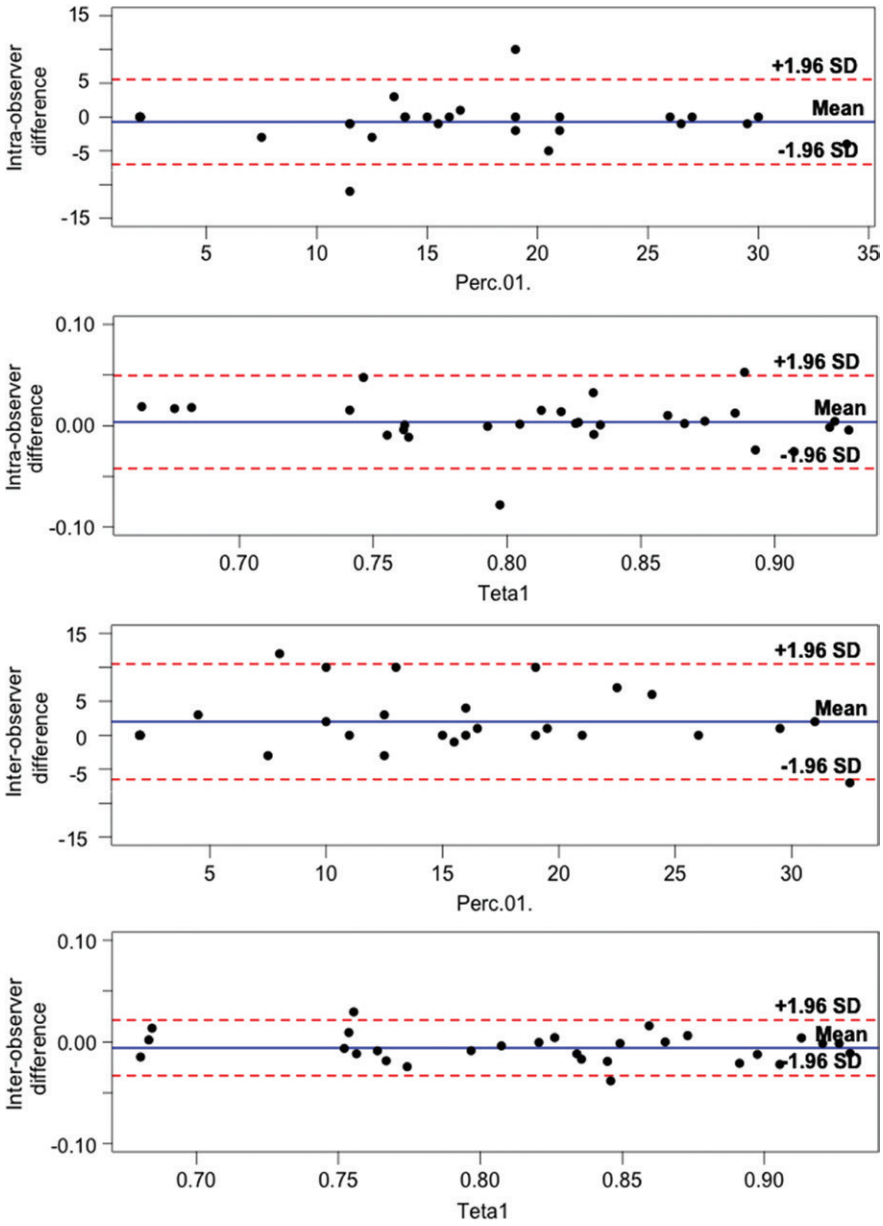

Figure 5: Bland-Altman plots illustrate intraobserver (upper row) and interobserver (lower row) variability of the parameters Perc.01 and Teta1 derived from TA. Solid blue lines indicate bias. Dotted red lines indicate limits of agreement (1.96 × standard deviation).

should elucidate the ability of TA to assess the size and transmurality of myocardial scars on nonenhanced images to further enhance the clinical relevance of TA in the setting of MI. In addition, future studies should aim to compare other emerging noncontrast-enhanced techniques such as native T1 mapping or feature tracking and elucidate whether either technique is superior to another, or whether a combination of several techniques might be the best approach for nonenhanced scar detection with MR imaging.

We must acknowledge the following study limitations. First, there were inherent drawbacks of the retrospective study design. Second, the influence of different acquisition parameters, sequences, field strengths, and MR imagers on TA features remains to be investigated. Third, we used a two-dimensional region of interest on short-axis images of the LV myocardium, which potentially influences orientation-dependent texture features. The inclusion of rotation invariant and three-dimensional texture features in future studies might provide a more robust classification (35). Finally, the software used is technically not able to combine different texture features to a parametric map. Thus, we were not able to show the extent of myocardial scar on parametric displays of the two identified features Teta1 and Perc.01.

In conclusion, our proof-of-concept study indicates that TA is feasible and allows for the diagnosis of small and large subacute and chronic ischemic scars on nonenhanced cine MR images with high accuracy.

Disclosures of Conflicts of Interest: B.B. disclosed no relevant relationships. **M.M.** disclosed no relevant relationships. **S.O.** disclosed no relevant relationships. **D.M.** disclosed no relevant relationships. **H.A.** disclosed no relevant relationships. **R.M.** disclosed no relevant relationships.

References

1. Mozaffarian D, Benjamin EJ, Go AS, et al. Heart disease and stroke statistics—2016 update: a report from the American Heart Association. Circulation 2016;133(4):e38–e360.
2. Jernberg T, Hasvold P, Henriksson M, Hjelm H, Thuresson M, Janzon M. Cardiovascular risk in post-myocardial infarction patients: nationwide real world data demonstrate the importance of a long-term perspective. Eur Heart J 2015;36(19):1163–1170.
3. Bonaca MP, Bhatt DL, Cohen M, et al. Long-term use of ticagrelor in patients with prior myocardial infarction. N Engl J Med 2015;372(19):1791–1800.
4. von Knobelsdorff-Brenkenhoff F, Schulz-Menger J. Cardiovascular magnetic resonance imaging in ischemic heart disease. J Magn Reson Imaging 2012;36(1):20–38.
5. Goetti R, Kozerke S, Donati OF, et al. Acute, subacute, and chronic myocardial infarction: quantitative comparison of 2D and

3D late gadolinium enhancement MR imaging. Radiology 2011;259(3):704–711.

6. Liu H, Yan L, Ma GS, et al. Association of chronic kidney disease and coronary artery disease in 1,010 consecutive patients undergoing coronary angiography. J Nephrol 2012;25(2):219–224.
7. Stromp TA, Leung SW, Andres KN, et al. Gadolinium free cardiovascular magnetic resonance with 2-point cine balanced steady state free precession. J Cardiovasc Magn Reson 2015;17:90.
8. Collidge TA, Thomson PC, Mark PB, et al. Gadolinium-enhanced MR imaging and nephrogenic systemic fibrosis: retrospective study of a renal replacement therapy cohort. Radiology 2007;245(1):168–175.
9. Castellano G, Bonilha L, Li LM, Cendes F. Texture analysis of medical images. Clin Radiol 2004;59(12):1061–1069.
10. Tourassi GD. Journey toward computer-aided diagnosis: role of image texture analysis. Radiology 1999;213(2):317–320.
11. Kim JH, Ko ES, Lim Y, et al. Breast cancer heterogeneity: MR imaging texture analysis and survival outcomes. Radiology 2017;282(3):665–675.
12. Ng F, Ganeshan B, Kozarski R, Miles KA, Goh V. Assessment of primary colorectal cancer heterogeneity by using whole-tumor texture analysis: contrast-enhanced CT texture as a biomarker of 5-year survival. Radiology 2013;266(1):177–184.
13. Hodgdon T, McInnes MD, Schieda N, Flood TA, Lamb L, Thornhill RE. Can quantitative CT texture analysis be used to differentiate fat-poor renal angiomyolipoma from renal cell carcinoma on unenhanced CT images? Radiology 2015;276(3):787–796.
14. Tiwari P, Prasanna P, Wolansky L, et al. Computer-extracted texture features to distinguish cerebral radionecrosis from recurrent brain tumors on multiparametric MRI: a feasibility study. AJNR Am J Neuroradiol 2016;37(12):2231–2236.
15. Tabari A, Torriani M, Miller KK, Klibanski A, Kalra MK, Bredella MA. Anorexia nervosa: analysis of trabecular texture with CT. Radiology 2017;283(1):178–185.
16. MacKay JW, Murray PJ, Kasmai B, Johnson G, Donell ST, Toms AP. MRI texture analysis of subchondral bone at the tibial plateau. Eur Radiol 2016;26(9):3034–3045.
17. Depeursinge A, Chin AS, Leung AN, et al. Automated classification of usual interstitial pneumonia using regional volumetric texture analysis in high-resolution computed tomography. Invest Radiol 2015;50(4):261–267.
18. Thornhill RE, Cocker M, Dwivedi G, et al. Quantitative texture features as objective metrics of enhancement heterogeneity in hypertrophic cardiomyopathy. J Cardiovasc Magn Reson 2014;16(Suppl 1):P351.
19. Amado LC, Gerber BL, Gupta SN, et al. Accurate and objective infarct sizing by contrast-enhanced magnetic resonance imaging in a canine myocardial infarction model. J Am Coll Cardiol 2004;44(12):2383–2389.
20. Heidary S, Patel H, Chung J, et al. Quantitative tissue characterization of infarct core and border zone in patients with ischemic cardiomyopathy by magnetic resonance is associated with future cardiovascular events. J Am Coll Cardiol 2010;55(24):2762–2768.
21. Materka A. Texture analysis methodologies for magnetic resonance imaging. Dialogues Clin Neurosci 2004;6(2):243–250.
22. Szczypiński PM, Strzelecki M, Materka A, Klepaczko A. MaZda—a software package for image texture analysis. Comput Methods Programs Biomed 2009;94(1):66–76.
23. Collewet G, Strzelecki M, Mariette F. Influence of MRI acquisition protocols and image intensity normalization methods on texture classification. Magn Reson Imaging 2004;22(1):81–91.
24. Xu JW, Suzuki K. Max-AUC feature selection in computer-aided detection of polyps in CT colonography. IEEE J Biomed Health Inform 2014;18(2):585–593.
25. Khan JN, Singh A, Nazir SA, Kanagala P, Gershlick AH, McCann GP. Comparison of cardiovascular magnetic resonance feature tracking and tagging for the assessment of left ventricular systolic strain in acute myocardial infarction. Eur J Radiol 2015;84(5):840–848.
26. R Core Team. R: A language and environment for statistical computing. Vienna, Austria: R Foundation for Statistical Computing. http://www.R-project.org/. Accessed February 13, 2016.
27. Kursa MB, Rudnicki WR. A deceiving charm of feature selection: the microarray case study. In: Czachórski T, Kozielski S, Stańczyk U, eds. Man-machine interactions 2. 5th ed. Berlin, Germany: Springer, 2011; 145–152.
28. Kuhn M. Caret. Classification and regression training. 6th ed. https://github.com/topepo/caret/. Accessed May 17, 2016.
29. Lücke C, Schindler K, Lehmkuhl L, et al. Prevalence and functional impact of lipomatous metaplasia in scar tissue following myocardial infarction evaluated by MRI. Eur Radiol 2010;20(9):2074–2083.
30. Rajiah P, Desai MY, Kwon D, Flamm SD. MR imaging of myocardial infarction. RadioGraphics 2013;33(5):1383–1412.
31. Abdel-Nasser M, Melendez J, Moreno A, Puig D. The impact of pixel resolution, integration scale, preprocessing, and feature normalization on texture analysis for mass classification in mammograms. Int J Opt 2016;2016:1–12.
32. Larroza A, Bodí V, Moratal D. Texture analysis in magnetic resonance imaging: review and considerations for future applications. In: Constantinides C, ed. Assessment of cellular and organ function and dysfunction using direct and derived MRI methodologies. Rijeka, Croatia: InTech, 2016.
33. Gillies RJ, Kinahan PE, Hricak H. Radiomics: images are more than pictures, they are data. Radiology 2016;278(2):563–577.
34. Mayerhoefer ME, Szomolanyi P, Jirak D, et al. Effects of magnetic resonance image interpolation on the results of texture-based pattern classification: a phantom study. Invest Radiol 2009;44(7):405–411.
35. Depeursinge A, Foncubierta-Rodriguez A, Van De Ville D, Müller H. Three-dimensional solid texture analysis in biomedical imaging: review and opportunities. Med Image Anal 2014;18(1):176–196.